PHYSICAL REVIEW E VOLUME 52, NUMBER 2 AUGUST 1995

Optical investigations in the various phases of an antiferroelectric liquid crystal

John Philip,* Jean René Lalanne, Jean Paul Marcerou, and Gilles Sigaud
Centre de Recherche Paul Pascal, CNRS, Avenue A. Schweitzer, 33600 Pessac, France

(Received 1 March 1995)

We report detailed results of optical rotatory power (ORP), slective reflection (SR), refractive index anisotropy (RIA), and anisotropic Rayleigh scattering (ARS) measurements in the antiferroelectric liquid crystal, 4-(1-methylheptyl-oxycarbonyl) phenyl-4′octyloxy phenyl-4-carboxylate (MHPOBC). The ORP in Sm-A and Sm-C_α^* phases has been found to be zero or at least very weak compared to ordinary liquids with strongly chiral molecules. No helical pitch is observed in the Sm-A, Sm-C_α^* and Sm-C_γ^* phases in the range 200–2200 nm. The combined use of ORP and SR allows the precise determination of the tilt angle of the smectic-C phases. Obtained values are found to be in good agreement with both theoretical calculations and experimental results obtained from RIA. Moreover, ARS reveals the local biaxial character of the Sm-C_A^* phase, while the absence of critical behavior of the Sm-$A \rightleftharpoons$Sm-C_α^* phase transition is a direct proof of the lack of biaxiality in the Sm-C_α^* phase.

PACS number(s): 61.30.−v, 78.20.−e, 78.35.+c, 64.70.Md

I. INTRODUCTION

The discovery of ferroelectric liquid crystals (LC) [1] has triggered lot of interest due to their technological applications as well as a keen interest in the fundamental understanding of these phases. Soon after the discovery of the smectic-O phase in (1-methyl)-heptylterpthalidene-bis amino cinnamate, which greatly resembles the smectic C_A phase with the molecules positionally disordered inside the layers and tilted relative to them, it has been known that the chiral O^* phase could be observed in ferroelectric samples [2–4]. In 1989, Chandani *et al.* synthesized a chiral compound 4-(1-methylheptyloxycarbonyl) phenyl-4′octyloxy phenyl-4-carboxylate (MHPOBC) which possesses four chiral smectic phases Sm-C_α^*, Sm-C^*, Sm-C_γ^*, and Sm-C_A^* [5]. This compound has been extensively studied during the last few years, in order to understand various properties and the structures of these relatively new chiral smectic phases [6–28]. Very recently, a review article has been published [29]. As a consequence of these rigorous efforts, the structure of the Sm-C^* phase has been clearly identified as ferroelectric. However, an understanding of the exact structures of the Sm-C_A^*, Sm-C_γ^*, and Sm-C_α^* phases is still in a premature stage.

The *Sm-C^* phase* (ferroelectric) is characterized by a chiral center which reduces its space symmetry to C_2, whereas its counterpart, the achiral smectic-C phase, has a C_{2h} symmetry. The ferroelectricity is expected to originate from the hindered rotation of the constituent molecules about their long axis, leading to an alignment of the transverse dipole moments of the constituent molecules perpendicular to the tilting plane, and thus to a macroscopic polarization within the smectic layers. Since the tilt occurs in the same direction in all layers, the smectic-C^* phase as a whole is ferroelectric in nature, irrespective to the slight precession from layer to layer, which is caused by the chiral center in the molecule. This leads to a helicoidal structure with the axis parallel to the layer normal.

The *Sm-C_A^* phase* (so called antiferroelectric) is assumed to be identical to the earlier discovered smectic-O^* phase, in which the tilt direction in adjacent layers alternates in the direction symmetrical with respect to the layer normal (herringbone structure) [3,4,27]. Racemic mixtures [4], or achiral compounds [27], exhibit Sm-O or Sm-C_A phases, miscible in any proportion to its Sm-O^* or Sm-C_A^* analog, proving that an eventual in-plane polarization, even if it has been observed when building thin films layer by layer [4], does not play a leading role in the structure of this phase. In summary, the Sm-C_A^* phase appears as a bilayered, tilted, nonferroelectric, and biaxial phase. The symmetry allows an alternate polarization in successive layers [4,26], but there is no requirement for its value to be equal to the spontaneous polarization (per layer) of the corresponding (same tilt angle θ) Sm-C^* phase.

The *Sm-C_γ^* phase,* (so called ferrielectric), is in several aspects intermediate between the Sm-C^* and Sm-C_A^* phases. In MHPOBC [23], it is separated from these phases by two weakly first order transitions and exhibits a finite weak permanent polarization, weaker than the one of the SmC^* phase, which reacts in characteristically peculiar ways to the external electric field, showing multistability in thin planar samples [11] or induced biaxiality in thick homeotropic samples [15]. Different models have been proposed in order to describe the Sm-C_γ^* phase from a mixture of an essentially monolayered Sm-C^* (tilt angle θ, azimuthal angle ϕ) and a bilayered Sm-$C_A^*(\theta_1=\theta_2$ and $\phi_2=\phi_1+\pi)$ phase. The same model [12], introducing different tilt angles θ_1 in adjacent layers, is not supported by x-ray scattering results [10], while oth-

---

*Present address: Metallurgy and Materials Science Division, Indira Gandhi Center for Atomic Research, Kalpekkam, 603102 Tamilnadu, India.

ers [5,28], introducing different azimuthal angles ($\phi_{i+1} \neq \phi_i$ and $\phi_{i+1} \neq \phi_i + \pi$), do not account for the conoscopic experimental observations under electric field [15]. The most reasonable models seem to be the multilayered ones ($\theta_{i+1} = \theta_i$, $\phi_{i+1} = \phi_i$, or $\phi_{i+1} = \phi_i + \pi$) which may possibly be described by a devil's staircase [21,24].

Interest at the present time is primarily focused on the Sm-C_α^* phase. Unfortunately, many of the experimental investigations were unsuccessful in deriving any information about the structure of this phase. For instance, it seems particularly difficult to observe the Sm-$A \rightarrow$Sm-C_α^* phase transition optically. As far as we know, the only incontestable result has been obtained from a high-resolution calorimetric study [23] which showed the Sm-$A \rightarrow$Sm-C_α^* phase transition and proved its second-order character. One must also note that, from the pretransitional effect observed in circular dichroism studies [14], it was prematurely concluded that Sm-C_α^* (as well as the Sm-A) phases possess helical structures. But this argument is not confirmed at the present time [29]. The same conclusion must be raised concerning the possible biaxial Sm-A character of the phase, previously advanced [14] (by biaxial Sm-A we mean an untilted biaxial phase where the layer normal is an eigenaxis for any 3×3 tensor).

As a result, the exact structure of the Sm-C_α^* phase remains unknown at this stage, except that it consists of a macroscopically uniaxial phase built with tilted molecules.

Although numerous articles have appeared in recent years about the properties of these phases, numerous published but unconfirmed (and sometimes invalidated) results exist in the literature, as well as many premature conclusions [30] and experimental deficiencies [31].

Four years ago, we decided to undertake correlated optical investigations of these phases using samples of (i) optical quality, (ii) various thicknesses, and (iii) different alignments (homeotropic or planar).

A test of the self-consistency of all these results, obtained from very different investigations and samples, could then be performed, and would clarify the already noticed discrepancies. Moreover, as a prerequisite in all optical experiments, we impose a step by step thermal stabilization of all our samples associated to very slow thermal scanning speeds (down to 50 mK per hour), to be sure to record physical properties at equilibrium.

Here we present the entire results of our investigations [32]. Section II is devoted to sample preparations, descriptions of the experimental setup, and the determination of the phase transition temperatures. We have used four optical techniques, namely anisotropic Rayleigh scattering (ARS), optical rotatory power (ORP), selective reflection (SR) and refractive index anisotropy (RIA). Section III presents and discusses the results. Finally Sec. IV concludes and gives perspectives of this work.

II. EXPERIMENTS

A. Samples and their preparation

High-purity (R)-MHPOBC [4-(1-methyleptyloxycarbonyl)phenyl 4′octyloxy-biphenyl-4-carboxylate] was obtained from private sources [33] and purchased from the Chisso Corporation, Japan. It was used without further purification. At the precision of our work, we never detected any difference between the samples obtained from these three different sources.

Homeotropically aligned samples of (100±5)-μm thickness (Hellma 210 003 QS) are prepared by coating the plates with octadecyl-triethoxy silane (ODS) and the sample is aligned in a magnetic field of about 1.4 T, by cooling slowly down from the isotropic phase. Planar samples of (7±1) μm are prepared from pretreated commercial cells (LINKHAM) and aligned by applying an electric voltage of about 20 V across the two electrodes of the cell. Before filling the cell with MHPOBC, an accurate value (a relative precision of about 0.01) of the thickness of the cell is measured by using interference phenomena due to the reflection of white light on the two inner surfaces of the plates.

The optical quality of the samples (an extinction ratio between crossed polarizers and spatial homogeneity) is checked by polarized microscopy [32].

B. Experimental setup

1. Anisotropic rayleigh scattering (ARS) and optical rotatory power (ORP)

The principle of ARS and ORP measurements is shown in Fig. 1. A He-Ne laser beam of wavelength 632.8 nm, with a very low power in order to avoid any

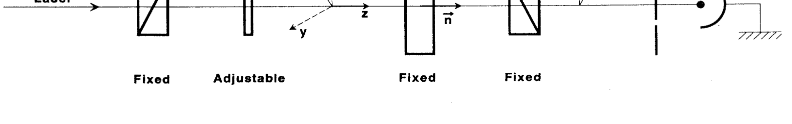

FIG. 1. Principle of the anisotropic Rayleigh scattering (ARS) and optical rotatory power (ORP) measurements: (a) At each temperature, the ORP of the sample is compensated by rotating the half-wave plate (→ORP). (b) After ORP compensation by the half-wave plate, the minimum value of the intensity at a fixed wave vector ($|\mathbf{q}| \cong 4.15 \times 10^2$ cm^{-1}) is recorded (→ARS).

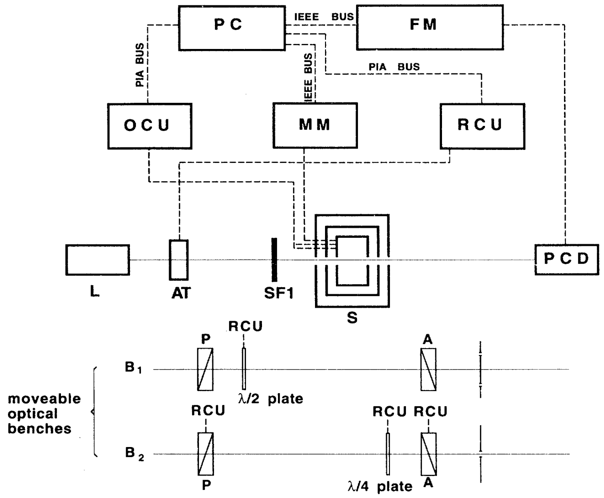

FIG. 2 Experimental setup for ARS, ORP, and RIA measurements; bench B_1 inserted: ARS+ORP; bench B_2 inserted: RIA. *L*: He-Ne laser (Uniphase model 1135*P*, $\lambda=632.8$ nm, $P=1$ mW); AT: motorized attenuator; *P*, *A*: polarizers; SF1: spatial filter ($\phi=7$ mm); *S*: sample oven; PCD: photon counting device (Hamamatsu C1050); FM: frequency meter (Philips PM 6665); RCU: rotation control unit; MM: multimeter (Philips PM2534); OCU: oven control unit; PC: IBM PS 8550.

heating (about 10^{-6} W inside the sample) is used for these investigations. The beam passes through the homeotropically aligned sample placed inside the oven. Here the molecules are oriented normal to the surface of the glass plates, with the director along the *Z* axis. The oven is mounted in such a way that the sample position can be adjusted to have the optic axis parallel to the wave vector of the incident laser beam. The analyzer *A* is in a crossed position with respect to the first polarizer *P*, with the output polarization along the *Y* axis. At each stabilized temperature, the rotation of the incoming beam polarization, due to the optical rotatory power of the sample, is compensated for by rotating the half-wave plate in the appropriate direction. Twice the angle θ rotated by the half-wave plate is a measure of ORP of the sample. When the ORP of the sample is fully compensated for by rotating the half-wave plate, the intensity of the light transmitted through the analyzer and the annular pinhole will have a minimum value which is a measure of the ARS intensity at a fixed wave vector given by the annular diaphragm ($q \approx 4.15\times10^2$ cm^{-1}).

The experiment is described in Fig. 2. The laser light intensity is stabilized (relative low frequency fluctuations less than 0.01) and continuously controlled by the computer unit PC variable attenuator (AT), thus providing a reference signal taking into account both the remaining fluctuations of the laser intensity and those coming from the photon counting device (PCD) coupled to the frequency meter (FM).

The half-wave plate is mounted on a microcontrolled rotation stage (RCU) which is interfaced with the computer. One step of the rotation is 0.01°. The half-wave plate is rotated in the right direction, where the intensity has a minimum value, in order to find the approximate minimum intensity. Then, with respect to this minimum, a parabola is plotted by taking five or more measurements on each side of the rough minimum, and the rotation stage is placed at this computed value of the minimum. A rotating cylinder (not shown in Fig. 2), placed in front of the PCD and driven by the RCU, allows signal and reference measurements separately. The temperature of the samples is maintained within 1 mK-long term stability by using a triple-walled (with two heating stages) especially designed oven, controlled by a computer. Using this oven, we were able to perform the experiments step by step, the smallest interval between the steps being 5 mK. The thermal stability of the sample was checked before each measurement.

2. *Refractive index anisotropy (RIA)*

The principle of the experiment is described in Fig. 3. The planar sample is in a fixed position. The polarizer (*P*), analyzer (*A*), and quarter-wave plate (*R*) were adjusted to have minimum transmitted intensity. At this position, the neutral lines of *R* are parallel to the principal axes of *P* and *A*, and the optic axis of the sample is also parallel to one neutral line of *R*. Then *P* and *R* are rotated by 45° in the same direction and the analyzer is adjusted to have a minimum transmitted intensity. The rotation angle of the analyzer is a measure of the ellipticity and hence of the RIA. The experimental setup is quite the same as the previous one (see Fig. 2). We only replace the optical bench B_1 by B_2, and detect the central part of the beam by using a pinhole of reduced diameter ($\varnothing\sim1$ mm). We then avoid a possible diffraction of the laser light by the medium.

3. *Selective reflection (SR)*

Selective reflection measurements have been carried out in a 100-μm-thick homeotropic sample, using an Oriel reflectometer (model 77400). The white light from the halogen lamp is sent through an optical fiber to the

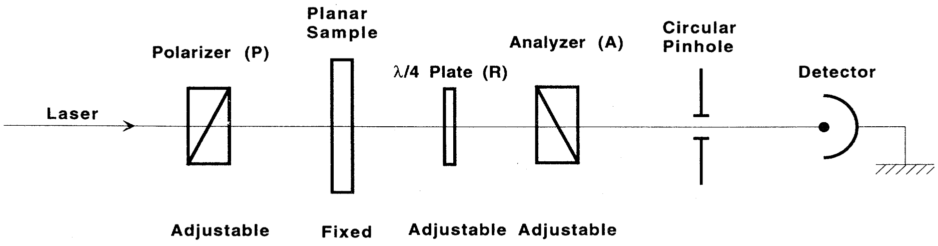

FIG. 3. Principle of the refractive index anisotropy (RIA) measurement.

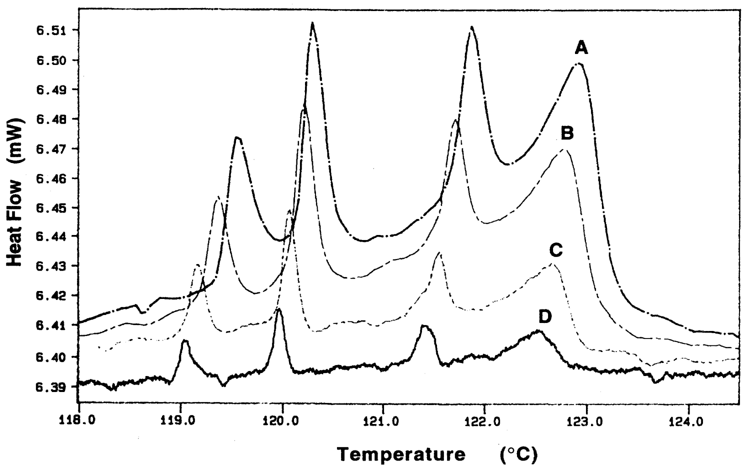

FIG. 4. Results of the differential scattering calorimetry (DSC); sample: (R)-MHPOBC (20 mg, disordered); cooling procedure; rates: A:2 K mn^{-1}; B:1 K mn^{-1}; C:0.5 K mn^{-1}; D+0.3 K mn^{-1}.

sample, which is mounted for normal incidence. The reflected light is again sent through another optical fiber to a spectrograph linked to a computer. The reflectance (%) as a function of wavelength (in the range 200–2200 nm) is then recorded for various stable temperatures. In this case, we use an oven with a thermal stability of ±0.01 K.

C. Phase transition temperature determination by differential scanning calorimetry (DSC)

As we already pointed out, the problem of accurate and reliable determination of the various phase transition temperatures is the most important one in these studies. It is sometimes quite difficult to observe all the phase transitions. For instance, calorimetric studies performed in both the ac and relaxation modes at rates about 1 mK h^{-1} give large discrepancies [23] with DSC results [9]: they only clearly show the Sm-$A \rightleftharpoons$Sm-C_α^* phase transition. On the other hand, we will see that this transition cannot be seen in all our optical investigations.

In order to overcome this difficulty, we have first performed DSC, using a Perkin-Elmer model DSC 7 calorimeter. The results for different rates are shown in Fig. 4. The phase transition temperatures are found to shift toward the low temperature side as the scanning speed is lowered, and are extrapolated at zero scanning speed.

Then we carefully calibrated all our thermometers with respect to the one used in DSC by using an auxiliary compound ($C_4H_9O\varphi CO_2\varphi COC_2H_5$), where ϕ indicates the aromaticizing, exhibiting a transition from nematic to isotropic at 121.4 °C, i.e., in the temperature range used for our experiments. Table I gives the different transition temperatures recorded in three different experiments (the case of the RIA in planar samples will be discussed in detail in Sec. III) performed on (R)-MHPOBC.

Good agreement can be noted between the results of the first three investigations. We must also point out that, in spite of the relatively high temperatures used here, the R-MHPOBC samples were found to be fairly stable, in agreement with previous observation [23]. We do not observe any drift larger than some cK during each run (some days). Of course, we always change the sample between two runs in order to avoid a possible aging of the compound under investigation. Let us now present and discuss the entire results.

TABLE I. Phase transition temperature (in °C) of (R)-MHPOBC recorded in our different experiments (all thermometers were previously calibrated with respect to the same reference sample).

Experiment	Sample	SmA ↓↑ SmC_α^*	SmC_α^* ↓↑ SmC^*	SmC^* ↓↑ SmC_γ^*	SmC_γ^* ↓↑ SmC_A^*	Precision of the temperature determination
DSC	20 mg disordered	122.5(0)	121.3(5)	119.8(0)	118.9(5)	± °C0.1
ARS + ORP	thickness: 100 μm homeotropic	?	121.30	119.80	118.90	±0.01
SR	thickness: 100 μm homeotropic	?	121.30	119.75	118.70	±0.05
RIA	thickness: ~7 μm planar	117.25	?	114.60	?	±0.01

III. RESULTS AND DISCUSSION

A. ORP, SR, and RIA

The physics of ORP and SR in liquid crystals were established, in the case of cholesterics, by De Vries [34]. An extensive literature devoted to this case has been already published [35]. More recently, these works were extended to the Sm-C^* phases [36,37]. They all assume that, in the chiral Sm-C^* phases, the molecular axis is uniformly rotated around the layer normal axis Z (see Fig. 5), with a tilt angle θ fixed at a value between 0° and 90°. The azimuthal angle is $\phi(z)=(2\pi/L)z$, where L is the helical pitch. So the orientation of the molecular axis as well as the components $\varepsilon(z)$ of the dielectric tensor functions of both θ and $\phi(z)$. The study of electromagnetic wave propagation along the helical axis in this periodic structure proves ORP and SR: when the product ($\lambda_0=Ln_{\text{eff}}$) of the helical pitch and the mean in-plane refractive index n_{eff} is much smaller than the wavelength λ of the incident wave, ORP tends to decay asymptotically to zero as L^3, while in the case $\lambda_0 \gg \lambda$ an ORP proportional to L is induced. When $\lambda_0 \approx \lambda$, Bragg scattering can occur and strong perturbation of the propagation appears: here a linearly polarized incident wave gives rise to two, respectively totally reflected and transmitted, circularly polarized components.

We have extended the already published results for the cholesteric and Sm-C^* phases to the case of the Sm-C_A^* phase which is considered in this work [38]. Moreover, de Vries' calculation of the ORP is based on the assumption that the anisotropy of the refractive index Δn (namely the difference between extraordinary and ordinary indexes in the Sm-A phase) is weak ($n\Delta n \ll 1$). In fact, this assumption is not exactly fulfilled in LC (for instance, Δn in the range 0.2–0.3 are often obtained in usual LC [39]). We also take this point into account.

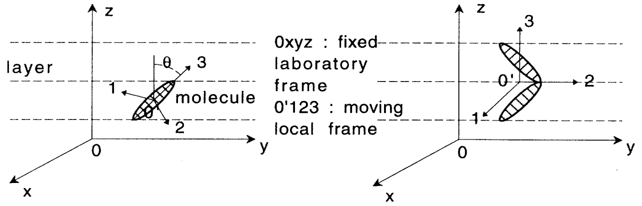

FIG. 5. Orientation of molecules in Sm-C^* and Sm-C_A^* phases. Sm-C^*: tilted biaxial phase in the local frame. From layer to layer, the molecular axis 3 is uniformly rotated around the layer normal 0z. Sm-C_A^*: untilted biaxial phase in the local frame with herringbone structure. From layer to layer, the molecular principal axes 01 and 02 are uniformly rotated around the fixed 03 axis always parallel to the layer normal 0z.

Figure 5 represents the two assumed microscopic structures of the Sm-C^* and Sm-C_A^* phases. These microscopic arrangements lead to strong differences in the expressions of the dielectric tensors in their principal frames 0'123:

$$\text{Sm-}C^*\text{(quasiuniaxial tensor): } \varepsilon_{\alpha\beta}=\begin{bmatrix} \varepsilon_\perp+0(\varepsilon_a) & & 0 \\ & \varepsilon_\perp & \\ 0 & & \varepsilon_\parallel-0(\varepsilon_a) \end{bmatrix}, \tag{1}$$

$$\text{Sm-}C_A^*\text{(biaxial tensor): } \varepsilon_{\alpha\beta}=\begin{bmatrix} \varepsilon_\perp+0(\varepsilon_a) & & 0 \\ & \varepsilon_\perp-0(\varepsilon_a)+\varepsilon_a\sin^2\theta & \\ 0 & & \varepsilon_\perp+\varepsilon_a\cos^2\theta \end{bmatrix}, \tag{2}$$

Here $\varepsilon_a=\varepsilon_\parallel-\varepsilon_\perp$. $0(\varepsilon_a)$ is a small positive number that we have evaluated, with the help of Ref. [15], to be about 10^{-2}, and that we neglect in the following.

Then, after a periodic rotation of period $L=2\pi/q$ (L is the pitch of the structure), and assuming that at $z=0$ (entrance of the sample) 0'3 is in the plane $x0z$, we obtain the following in the fixed laboratory frame.

For the Sm-C^* phase,

$$\varepsilon_{ij}(z)=\begin{bmatrix} \varepsilon_\perp+\frac{1}{2}\varepsilon_a\sin^2\theta & & 0 \\ & \varepsilon_\perp+\frac{1}{2}\varepsilon_a\sin^2\theta & \\ 0 & & \varepsilon_\perp+\varepsilon_a\cos^2\theta \end{bmatrix} + \frac{1}{2}\varepsilon_a\sin^2\theta\begin{bmatrix} \cos2qz & \sin2qz & 0 \\ \sin2qz & -\cos2qz & 0 \\ 0 & 0 & 0 \end{bmatrix} + \frac{1}{2}\varepsilon_a\sin2\theta\begin{bmatrix} 0 & 0 & \cos qz \\ 0 & 0 & \sin qz \\ \cos qz & \sin qz & 0 \end{bmatrix}, \tag{3}$$

and, for the Sm-C_A^* phase,

$$\varepsilon_{ij}(z)=\begin{bmatrix} \varepsilon_\perp+\frac{1}{2}\varepsilon_a\sin^2\theta & & 0 \\ & \varepsilon_\perp+\frac{1}{2}\varepsilon_a\sin^2\theta & \\ 0 & & \varepsilon_\perp+\varepsilon_a\cos^2\theta \end{bmatrix} + \frac{1}{2}\varepsilon_a\sin^2\theta\begin{bmatrix} \cos2qz & \sin2qz & 0 \\ \sin2qz & -\cos2qz & 0 \\ 0 & 0 & 0 \end{bmatrix}. \tag{4}$$

The last term of Eq. (3) is now missing, in agreement with the assumed structure of Sm-C_A^*, which supposes that 0z is one of its principal axes.

In ORP experiments, the laser beam propagates a plane wave with a wave vector parallel to the normal of the layers 0z (see Fig. 5, normal incidence). It has been previously shown [37] that two eigenmodes—each consisting of two circularly polarized plane waves—exist. The main result is that, except in the close vicinity of $\lambda_0=\lambda$, ORP is given by

$$\rho=-\pi\frac{\varepsilon_{a,\mathrm{eff}}^2\sin^4\theta\lambda_0^3}{16n_{\mathrm{eff}}^3\lambda^2(\lambda_0^2-\lambda^2)} . \tag{5}$$

ρ is the optical rotation per unit length (we assumed that $\rho \ll L$), θ is the tilt angle, and n_{eff} is an effective mean refractive index in the layer plane given by the following.

In Sm-C^*,

$$n_{\mathrm{eff}}^2=\varepsilon_\perp\left[1+\frac{(\varepsilon_a/\varepsilon_\perp)\sin^2\theta}{2[1+(\varepsilon_a/\varepsilon_\perp)\cos^2\theta]}\right] . \tag{6}$$

In Sm-C_A^*,

$$n_{\mathrm{eff}}^2=\varepsilon_\perp\left[1+\frac{\varepsilon_a}{2\varepsilon_\perp}\sin^2\theta\right] . \tag{7}$$

$\varepsilon_{a,\mathrm{eff}}$ is an effective anisotropy of the dielectric tensor given by the following.

In Sm-C^*,

$$\varepsilon_{a,\mathrm{eff}}=\frac{\varepsilon_a\varepsilon_\perp}{\varepsilon_\parallel-\varepsilon_a\sin^2\theta} . \tag{8}$$

In Sm-C_A^*,

$$\varepsilon_{a,\mathrm{eff}}=\varepsilon_a . \tag{9}$$

We must note that, in the case of small anisotropy $\varepsilon_a/\varepsilon_\perp \ll 1$, the distinction between formulas relative to the two phases disappears, and Eq. (5) leads to

$$\rho\approx-\pi\frac{L\Delta n_{\mathrm{Sm}\text{-}A}^2\sin^4\theta}{4\lambda^2[1-(\lambda/\lambda_0)^2]} , \tag{10}$$

with

$$\Delta n_{\mathrm{Sm}\text{-}A}=n_\parallel-n_\perp=\sqrt{\varepsilon_\parallel}-\sqrt{\varepsilon_\perp} , \tag{11}$$

which is exactly the result already obtained by de Vries [34] and Ong [37]. In fact, the correcting term distinguishing Sm-C^* and Sm-C_A^* phases is $\varepsilon_\perp/(\varepsilon_\perp+\varepsilon_a\cos^2\theta)=1/(1+\varepsilon_a/\varepsilon_\perp\cos^2\theta)$. With the usual values $n_\parallel\approx1.7$, $n_\perp\approx1.5$ [39,15], and $\theta\approx10°$ [40], ε_a is about 0.64 and $\varepsilon_a\cos^2\theta/\varepsilon_\perp\approx0.3$. This correction cannot be neglected as we discuss experimental results obtained in the various phases of MHPOBC.

In SR experiments, we directly measure λ_0 at various temperatures (i) when selective reflection really occurs in the studied phase and (ii) when λ_0 is included in the wavelength range of detection allowed by the experimental setup.

In RIA experiments performed in planar samples, the long molecular axis is, in the Sm-A phase, assumed to be parallel to the 0z axis (see Fig. 5). In other phases, the helix axis (if it exists) is in the 0z direction (see Fig. 5). The light wave propagates along 0x and probes the difference $\Delta n_{\mathrm{exp}}=\sqrt{\varepsilon_{zz}}-\sqrt{(\varepsilon_{xx}+\varepsilon_{yy})/2}$ of the components of the dielectric tensor given by Eqs. (3) or (4). We immediately see that the distinction between SmC^* and SmC_A^* phases in the ORP description is unnecessary. In the two cases we obtain

$$\begin{aligned}\varepsilon_{zz}&=\varepsilon_\parallel-\varepsilon_a\sin^2\theta=n_{\mathrm{max}}^2 ,\\(\varepsilon_{xx}+\varepsilon_{yy})/2&=\varepsilon_\perp+(\varepsilon_0/2)\sin^2\theta=n_{\mathrm{min}}^2 ,\end{aligned} \tag{12}$$

which leads to a measured anisotropy of the reflective index Δn_{exp} given by

$$\begin{aligned}\Delta n_{\mathrm{exp}}&=n_{\mathrm{max}}-n_{\mathrm{min}}\\&=[(n_\parallel^2-n_\perp^2)/(n_{\mathrm{max}}+n_{\mathrm{min}})](1-\tfrac{3}{2}\sin^2\theta) .\end{aligned} \tag{13}$$

When $\varepsilon_a/\varepsilon_\perp \ll 1$, Eq. (13) leads to

$$\Delta n_{\mathrm{exp}}\approx\Delta n_{\mathrm{Sm}\text{-}A}(1-\tfrac{3}{2}\sin^2\theta) , \tag{14}$$

an asymptotic and simpler expression valid only in the hypothetical case of very weak anisotropy.

In all our studies, we use the general relations (5) and (13): we measure $\Delta n_{\mathrm{Sm}\text{-}A}$ and λ_0, respectively, by RIA and SR techniques. An auxiliary measurement of $\bar{n}=(n_\parallel+2n_\perp)/3$ allows the determination of $n_\parallel$, $n_\perp$, $\varepsilon_\parallel$, $\varepsilon_\perp$, and ε_a. Then we can check the self-consistency of our different experimental results by using the general relations given by Eqs. (5) and (13) and, if successful, obtain physical parameters for the structures and their thermal variations.

The ORP results are presented in Fig. 6. In the two phases Sm-A and Sm-C_α^*, ORP is less than 0.2° mm^{-1} (zero or at least smaller than that of ordinary liquids with chiral molecules [41]). By using Eq. (5), we can calculate the smallest value of λ_0 ($\lambda_{0,\mathrm{min}}$), leading to a possible experimental detection of ORP (0.1° mm^{-1}). With the usual values already cited and with $\theta\sim7°$ (at the low temperature edge of the Sm-C_α^* phase) we find $\lambda_{0,\mathrm{min}}\approx310$ nm, corresponding to a minimal pitch $L_{\mathrm{min}}\approx207$ nm.

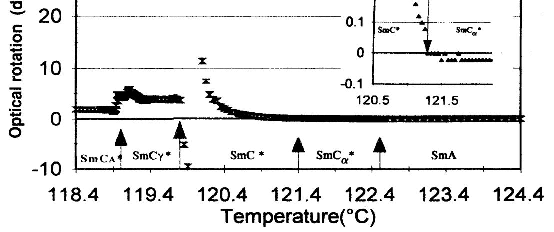

FIG. 6. The overall variation of optical rotation as a function of temperature in (R)-MHPOBC [homeotropic sample; thickness (100±5) μm].

This very small pitch is, of course, very difficult to detect. But this result does not contradict a previous qualitative conclusion [14] deduced from circular dichroism at 360 nm in this compound, and which assumes the existence of a helix in the Sm-A and Sm-C_α^* phases.

No pretransitional effect is observed at the second-order Sm$A \rightleftharpoons$Sm-C_α^* phase transition. However, such a pretransitional effect has already been reported [42,43] in the vicinity of the Sm-$A \rightleftharpoons$Sm-C^* phase transition in p-(n)-decyloxy-benzylidene)-p-amino-(2-methylbutyl) cinnamate (DOBAMBC), which exhibits an ORP of a few deg mm^{-1} in the Sm-C^* phase (the same order of magnitude as MHPOBC). This experimental result is probably linked to the zero or very weak value of the pitch in the Sm-C_α^* phase.

The inset in Fig. 6 exhibits a finite jump in ORP of about 0.1° (ten times larger than the experimental uncertainty) at the Sm-$C_\alpha^* \rightleftharpoons$Sm-$C^*$ phase transition, in agreement with the unchallenged existence of a helix in the ferroelectric phase. ORP then increases as the temperature decreases, and changes its sign between 119.90 and 119.95 °C. At this temperature $\lambda_0 = 632.8$ nm. ORP then exhibits another finite jump at the Sm-$C^* \rightarrow$Sm-C_γ^* phase transition.

In the Sm-C_γ^* phase, a large and noisy signal is recorded. However, a polarizing microscope observation undoubtfully reveals the bad orientation of the sample [32]. Thus the signal may include some contribution coming from birefringence and must be considered as an apparent ORP. At last, the well-oriented Sm-C_A^* phase exhibits an ORP of about 20° mm^{-1} in its high temperature edge.

The SR results (obtained from different runs using both reflectometer and spectrograph) are presented in Figs. 7 and 8. SR occurs in the visible range in the whole Sm-C^* phase. We note that $\lambda_0 = 632$ nm for $t = 119.82$ °C, a value close to the one (119.92±0.02) obtained in the ORP experiment. In the Sm-C_A^* phase, SR lies in the near infrared range and increases quickly as temperature decreases, in good agreement with previous observations [10], proving a divergence of the pitch at low temperature. Finally, let us point out that we never detected SR phenomena (in our experimental range 200–2200 nm) in either Sm-C_α^* and Sm-C_γ^* phases, confirming the absence of detectable ORP in the Sm-C_α^* phase, as well as Fukuda's prediction ($\lambda_0 \sim 3.3$ μm) in the SmC_γ^* phase [14].

Combined results of ORP and SR reveal two facts.

(i) They allow us qualitatively to picture both the thermal variation and the signs of the ORP (ρ) and SR wavelengths (λ_0) in all phases (see Fig. 9): we can also determine the sign of the helix: in the temperature range explored, the only inversion (from left handed to right handed) occurs at the Sm-$C^* \rightarrow$Sm-C_γ^* phase transition, and not at the transition to Sm-C_A^*, contrary to the previous report [10].

(ii) By using Eqs. (5)–(9) we can accurately determine the thermal variation of the tilt angle θ in Sm-C^* and Sm-C_A^* phases. We have used $n_\parallel = (1.70 \pm 0.01)$, $n_\perp = (1.51 \pm 0.01)$, $\varepsilon_\parallel = n_\parallel^2 = (2.89 \pm 0.02)$, and $\varepsilon_\perp = (2.28 \pm 0.02)$, obtained from the experimental values $n_\parallel - n_\perp = (0.191 \pm 0.001)$, (the RIA measurement) and $\bar{n} = (1.573 \pm 0.007)$ (the measurement of the mean refractive index in the isotropic phase).

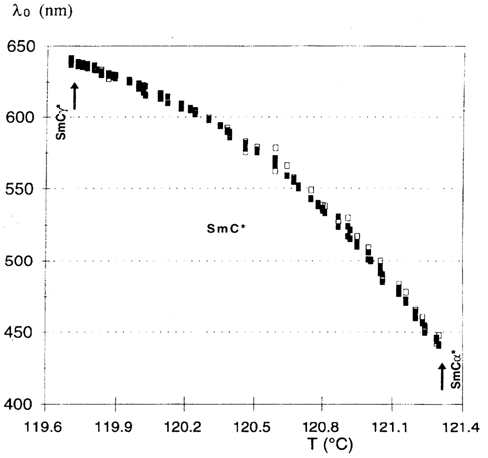

FIG. 7. The SR wavelength as a function of temperature in the SM-C^* phase of (R)-MHPOBC [homeotropic: (100±5)-μm-thick sample]; different dots represent different runs.

All these data are obtained at $\lambda = 632.8$ nm. The results are shown in Fig. 10. We have included two previously published results coming from conoscope observation without applied electric field [15] and electro-optic investigation [40]. We may notice that a relatively large dispersion of the results (by almost a factor of 2). In the latter case, the sample in Sm-C^* is induced by the electric field at any temperature, and large differences appear. We have also plotted the calculated values of $\sin^2\theta$ using Eq. (10), i.e., in the de Vries–Ong approximation: the discrepancy with Eq. (5) is in the range 10–20 %.

The RIA results are reported in Fig. 11. Three observations are made.

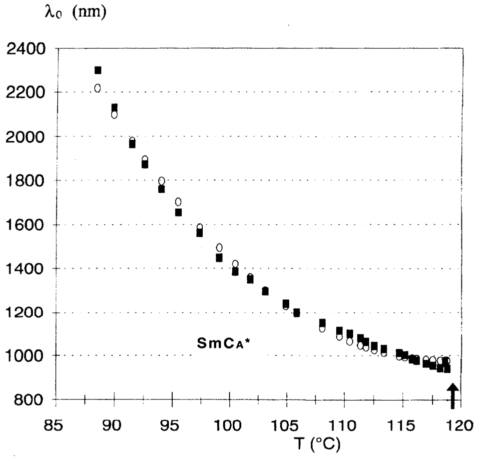

FIG. 8. The SR wavelength as a function of temperature in the Sm-C_A^* phase of (R)-MHPOBC [homeotropic: (100±5)-μm-thick sample]; different dots represent different runs.

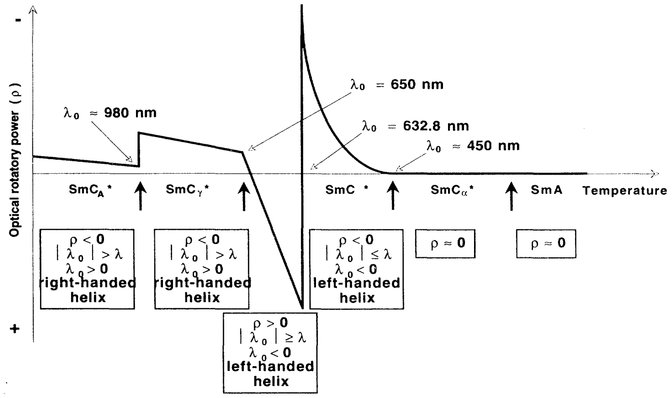

FIG. 9. Qualitative variation of ORP (ρ) and SR wavelengths (λ_0) vs temperature (ρ is assumed to be positive when an observer, placed at the level of the sample and looking toward the light source, observes a right-handed rotation of the polarization); compound: homeotropic (R)-MHPOBC; wave vector of the light parallel to the normal of the layers.

(i) A large shift ($\sim$5.2 K) appears at the Sm-$A \rightarrow$Sm-C_α^* phase transition, which occurs now at 117.25 °C. This may be due to the strong planar surface anchoring, already observed in the thin planar sample [44,45], and is more generally connected to the recent interesting results observed in thin films [46] and confined geometries [47].

(ii) A slight discontinuity of the experimental points appears 2.65 K below the Sm-$A \rightarrow$Sm-C_α^* phase transition temperature, corresponding to the difference of 2.70 K observed in DSC between Sm-$A \rightarrow$Sm-C_α^* and Sm-$C^* \rightarrow$Sm-C_γ^* phase transition temperatures (see Table I). It corresponds to the Sm-$C^* \rightarrow$Sm-C_γ^* transition. This observation is not fortuitous because (a) we observe it in each run (performed with different samples), and (b) it also appears in Fig. 4 of Ref. [40]. It seems linked to the misalignment in the Sm-C_γ^* phase which, in the case of thin samples, leads to a demixtion between ferroelectric and antiferroelectric microdomains [48], and can perhaps perturb RIA investigations at lower temperature.

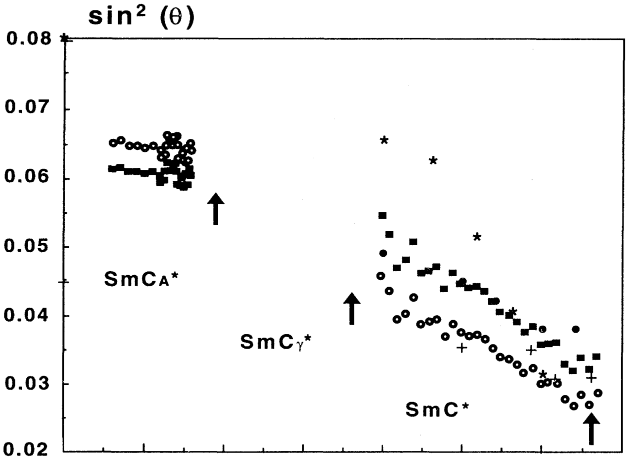

FIG. 10. Estimated values of $\sin^2\theta$ vs temperature; sample MHPOBC (R); (100±5)-μm thickness for ORP and RS (homeotropic geometry); (6.28±0.02)-μm thickness for RIA (planar geometry). ■, from our ORP and RS results, Eq. (5). ○, from our ORP and RS results, Eq. (10). ●, from our RIA results, Eq. (13). +, from Ref. [15], conoscope observation. *, from Ref. [40], electro-optic study.

(iii) The measured anisotropy in the Sm-A phase is about (0.191±0.001), larger than the one obtained from conoscope observation [15].

By using Eq. (13) we have calculated $\sin^2\theta$ versus temperature. The results are shown in Fig. 12, and confronted with the data given by ORP and SR in Fig. 10. They are in rather good agreement with these, showing the self-consistency of results given by very different optical techniques and sample alignments. Moreover, they permit us to validate our treatment of ORP without the de Vries-Ong approximation of weak anisotropy, which is not fulfilled in the case of MHPOBC ($\varepsilon_a \sim 0.6$ does not obey $\varepsilon_a \ll 1$).

B. ARS

ARS mainly reveals the in-plane (XY shown in Fig. 1) orientational fluctuations. These fluctuations generate Rayleigh scattering of a light wave with a wave vector along the OZ axis. They are related to fluctuations of the dielectric tensor ε_{ij} associated with the sample according to the following relation:

$$I_{XY}(\mathbf{q}_s) \sim \langle |\delta\varepsilon_{XY}(\mathbf{q}_s)|^2 \rangle \; , \qquad (15)$$

where $\varepsilon_{XY}(\mathbf{q}_s)$ is the Fourier transform of $\varepsilon_{XY}(\mathbf{r})$, I_{XY} is

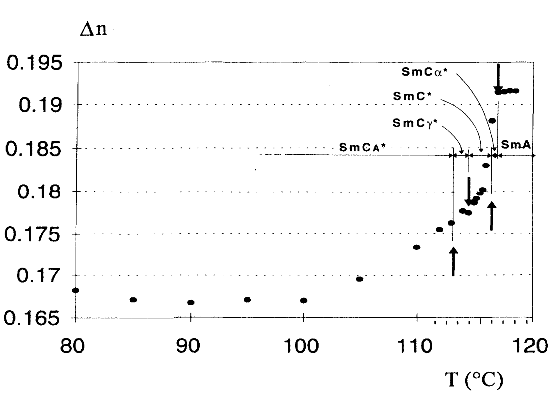

FIG. 11. RIA results; sample: (R)-MHPOBC; planar geometry; thickness: (6.28±0.02) μm; electric-field-induced alignment.

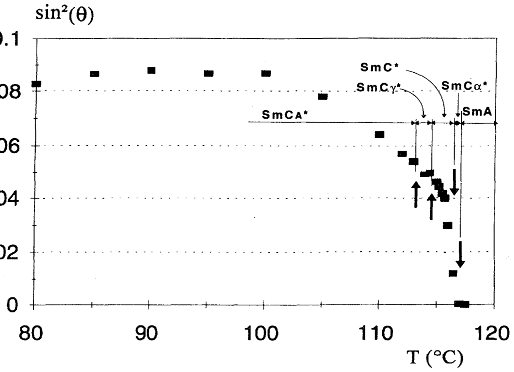

FIG. 12. Variation of $\sin^2\theta$ (θ: tilt angle) vs temperature from RIA results; sample: (R)-MHPOBC; planar geometry; thickness: (6.28±0.02) μm; electric-field-induced alignment.

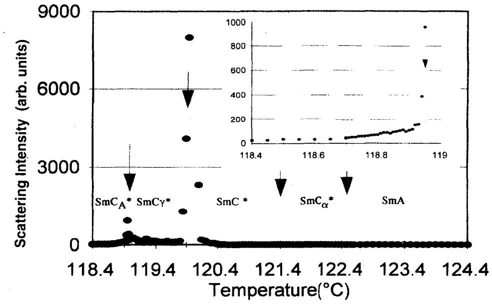

FIG. 13. The overall variation of ARS as a function of temperature in (R)-MHPOBC; homeotropic geometry; thickness: (100±5) μm; inset: enlarged view of the Sm-C_A^* phase.

the XY component of the scattering intensity, and $\mathbf{q}_s$ the scattering wave vector. The theoretical and experimental studies [49,50] on the XY components of the ARS in Sm-A phases have been performed in the vicinity of the transition to Sm-C. The $I_{XY}(\mathbf{q}_s)$ scattering intensity consists of two contributions, which can be written as follows:

$$I_{XY}(\mathbf{q}_s) \sim \varepsilon_a^2 \langle |j_{XY}(\mathbf{q}_s)|^2 \rangle + \langle |\Delta\varepsilon_{XY}^{(B)}(\mathbf{q}_s)|^2 \rangle \ . \tag{16}$$

$j_{XY}(\mathbf{q}_s)$ is an integral involving orientational variables in the laboratory frame and linking both the fluctuating director of the phase and the normal of the layer. $\Delta\varepsilon_{XY}^{(B)}(\mathbf{q}_s)^2$ describes the local biaxial character of the phase. Then the first term $\varepsilon_a^2 \langle |j_{XY}(\mathbf{q}_s)^2| \rangle$ is directly connected to the orientational fluctuations of the director of the phase, while the second one $\langle |\Delta\varepsilon_{XY}^{(B)}(\mathbf{q}_s)^2| \rangle$ is a local term introducing the local biaxial properties of the sample. It has been shown that, in classical Sm-A phases, (i) the first term is largely dominant (absence of local biaxial character), and (ii) it has a flat thermal behavior down to 10^{-2} K close to the Sm-$A \rightarrow$Sm-C phase transition, in agreement with theoretical predictions. Then ARS investigations could be a well adapted tool for the study of the biaxial-properties in MHPBC: the second term of Eq. (16) is expected to diverge in the vicinity of the phase transition between two locally uniaxial and biaxial phases, whereas the first term must show a flat background in this region.

The ARS experimental results are reported in Fig. 13. They have been corrected for thermal variations of the transmission of the sample pictured in Fig. 14. This transmission is quite flat (within 10%) except in the vicinity of the selective reflection phenomenon (119.92±0.02) where a reduction of about $\frac{1}{2}$ must be noted, in agreement with the physics of the phenomenon predicting the backward reflection of one of the two incident circular waves. This effect is of course responsible for the large signal observed in ARS at 119.29 °C (see Fig. 13), corresponding to the transformation of the linear polarized incident wave to a circularly polarized one passing through the linear analyzer (A) in Fig. 1.

Two main facts must be pointed out.

(i) We do not detect any divergence of ARS in the vicinity of the Sm-$A \rightarrow$Sm-C_α^* phase transition, reported to be of second order [23]. This is a clear indication of the nonexistence of local biaxial character of the Sm-C_α^* phase, which appears to be locally uniaxial, in contradiction with already published reports [11,14], but in agreement with recent prediction [21] involving, in this phase, a finite azimuthal correlation length smaller than the light wavelength.

(ii) As approaching the Sm-$C_A^* \rightarrow$Sm-C_γ^* phase transition from the left (see the inset in Fig. 13), we observe an increase (by at least a factor of 18) of the ARS signal, followed by an intense peak at the phase transition. This increase cannot be due to selective reflection (λ_0 is far from the 632.8-nm value in this region). Moreover, it cannot be explained by the thermal variations of λ_0, which are of very small amplitude in the vicinity of the phase transition. It seems more probably linked to the divergence of the second term in the right member of Eq. (16) and reveals a *biaxial-uniaxial phase transition* likely to appear.

One must note that a major difficulty for ascertaining such a hypothesis comes from the fact that the high temperature side of the transition cannot be studied: large fluctuations of both ARS and ORP signals occur, due to the poor alignment obtained in the Sm-C_γ^* phase. However, recent results performed on the related compound (R)-MHPBC exhibit the same divergence of ARS at the Sm-$C_\alpha^* \rightarrow$Sm-C_A^* phase transition between the two well aligned phases.

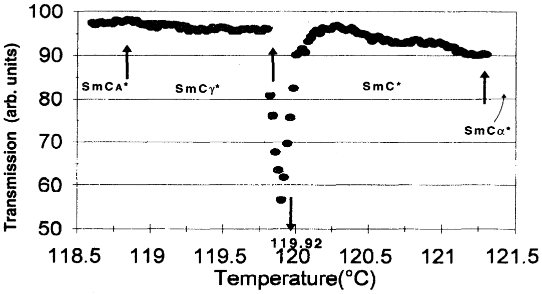

FIG. 14. Transmission of (R)-MHPOBC (homeotropic alignment); thickness: (100±5) μm; λ=632.8 nm; wave vector of the light parallel to the layer normal.

IV. CONCLUSION AND PERSPECTIVES

We have shown how precise ORP and SR investigations can lead to accurate estimations of the tilt angles in both Sm-C^* and Sm-C_A^* phases. We also proved that the anisotropy of the dielectric constant cannot be neglected in the calculations. Moreover, we have shown that results obtained by dielectric investigation under an applied electric field lead to largely different tilt angles, especially in the Sm-C_A^* phase: the tilt angle must not be considered to depend only on the temperature but also on the structure of the phase.

The Sm-C_α^* phase does not reveal any helicoidal structure in the visible and near-IR range. If it exists, the pitch is very small. We have not detected any biaxial character at the borders of the phase. It appears to be very difficult to distinguish Sm-C_α^* from Sm-A phases by using ORP or SR (while the Sm-$A \rightarrow$Sm-C_α^* transition is the transition easily detected by calorimetry).

Let us also point out that ARS has unambiguously established the biaxial character of the Sm-C_A^* phase, which appears to be optically equivalent to a chiral biaxial Sm-A phase, as proposed four years ago for the correlated Sm-O^* phase of MHTAC.[4] Then the natural perspectives of this work include the investigation of uniaxial-biaxial transitions, for instance, of Sm-$C_\alpha^* \rightarrow$Sm-C_A^* and Sm-$A \rightarrow$Sm-C_A^* phase transitions, which have very recently been shown to exist in related compounds [29].

ACKNOWLEDGMENTS

We are grateful to Professor Atsuo Fukuda and J. Prost for their constant encouragements, as well as to J. J. Piaud for his help during this work. We also thank Dr. H. T. Nguyen, Chisso Corporation, and Showa Shell Sekiyu, K. K., for providing us with the samples.

---

[1] R. B. Meyer, L. Liebert, L. Strzelecki, and P. Keller, J. Phys. Lett. **36**, L69 (1975).

[2] A. M. Levelut, C. Germain, P. Keller, L. Liebert, and J. Billard, J. Phys. **44**, 623 (1983).

[3] Y. Galerne and L. Liebert, Phys. Rev. Lett. **64**, 906 (1990).

[4] Y. Galerne and L. Liebert, Phys. Rev. Lett. **66**, 2891 (1991).

[5] A. D. L.Chandani, T. Hagiwara, Y. Suzuki, Y. Ouchi, H. Takezoe, and A. Fukuda, Jpn. J. Appl. Phys. **27**, L729 (1988).

[6] A. D. L. Chandani, Y. Ouchi, H. Takezoe, and A. Fukuda, Jpn. J. Appl. Phys. **27**, L276 (1988).

[7] M. Johno, A. D. L. Chandani, Y. Ouchi, H. Takezoe, A. Fukuda, M. Ichibashi, and K. Furukawa, Jpn. J. Appl. Phys. **28**, L119 (1989).

[8] M. Fukui, H. Orihara, Y. Yamada, N. Yamamoto, and Y. Ishibashi, Jpn. J. Appl. Phys. **28**, L849 (1989).

[9] A. D. L. Chandani, Y. Ouchi, H. Takezoe, A. Fukuda, K. Terashima, K. Furukawa, and A. Kishi, Jpn. J. Appl. Phys. **28**, L1261 (1989).

[10] A. D. L. Chandani, E. Gorecka, Y. Ouchi, H. Takezoe, and A. Fukuda, Jpn. J. Appl. Phys. **28**, L1265 (1989).

[11] K. Hiraoka, Y. Taguchi, Y. Ouchi, H. Takezoe, and A. Fukuda, Jpn. J. Appl. Phys. **29**, L103 (1990).

[12] H. Orihara and Y. Ishibashi, Jpn. J. Appl. Phys. **29**, L115 (1990).

[13] A. Suzuki, H. Orihara, Y. Ishibashi, Y. Yamada, N. Yamamoto, K. Mori, K. Nakamura, Y. Suzuki, T. Hagiwara, I. Kawamura, and M. Fukui, Jpn. J. Appl. Phys. **29**, L336 (1990).

[14] J. Lee, Y. Ouchi, H. Takezoe, A. Fukuda, and J. Watanabe, J. Phys. Condens. Matter **2**, SA271 (1990).

[15] E. Gorecka, A. D. L. Chandani, Y. Ouchi, H. Takezoe, and A. Fukuda, Jpn. J. Appl. Phys. **29**, 131 (1990).

[16] Y. Takanishi, K. Hiraoka, V. K. Agarwal, H. Takezoe, A. Fukuda, and M. Matsushita, Jpn. J. Appl. Phys. **30**, 2023 (1990).

[17] H. Takezoe, J. Lee, Y. Ouchi, and A. Fukuda, Mol. Cryst. Liq. Cryst. **202**, 85 (1991).

[18] T. Isozaki, Y. Suzuki, I. Kawamura, K. Mori, N. Yamamoto, Y. Yamada, H. Orihara, and Y. Ishibashi, Jpn. J. Appl. Phys. **30**, L1573 (1991).

[19] H. Sun, H. Orihara, and Y. Ishibashi, J. Phys. Soc. Jpn. **60**, 4175 (1991).

[20] T. Isozaki, T. Fujikawa, H. Takezeo, A. Fukuda, T. Hagiwara, Y. Suzuki, and I. Kawamura, Jpn. J. Appl. Phys. **31**, L1435 (1992).

[21] T. Isozaki, T. Fujikawa, H. Takezeo, A. Fukuda, T. Hagiwara, Y. Suzuki, and I. Kawamura, Phys. Rev. B **48**, 13 439 (1993).

[22] K. H. Kim, Y. Takaanishi, K. Ishikawa, H. Takezoe, and A. Fukuda, Liq. Cryst. **16**, 185 (1994).

[23] K. Ema, H. Yao, I. Kawamura, T. Chen, and C. W. Garland, Phys. Rev. E **47**, 1203 (1993).

[24] R. Bruinsma and J. Prost, J. Phys. (France) II, **4**, 1209 (1994).

[25] I. Musevic, R. Blinc, B. Zeks, M. Copic, M. M. Wi Hebrood, Th. Rasing, H. Orihara, and Y. Ishibashi, Phys. Rev. Lett. **71**, 1180 (1993).

[26] Ch. Bahr and D. Fliegner, Phys. Rev. Lett. **70**, 1842 (1993); Ch. Bahr, D. Fliegner, C. J. Booth, and J. W. Goodby, Europhys. Lett. **26**, 539 (1994).

[27] F. Hardouin, H. T. Nguyen, and A. M. Levelut, J. Phys. Lett. **43**, 779 (1982); L. Benguigui and F. Hardouin, *ibid.* **45**, 179 (1984).

[28] V. L. Lorman, A. A. Bulbitch, and P. Toledano, Phys. Rev. E **49**, 1367 (1994).

[29] A. Fukuda, Y. Takanishi, T. Isozaki, K. Ishikawa, and H. Takezoe, J. Mater. Chem. **4**, 997 (1994).

[30] For instance, the conclusions obtained from experiments performed on thin films are sometimes extended without care to the bulk properties.

[31] For instance, the very large differences of the (Sm-A+Sm-C) phase extensions noted in two studies of MHPOBC samples (whole extensions of the Sm-A, Sm-C_α^*, Sm-C^*, and Sm-C_γ^* phases of 4.3° in the DSC experiment, to be compared to 3.7° in the conoscopic observation performed on the 140-μm homeotropic sample).

[32] Some preliminary results can be found in J. Philip, J. R. Lalanne, J. P. Marcerou, and G. Sigaud, J. Phys. (France)

II, **4**, 2149 (1994).

[33] *R*-MHPOBC samples have been kindly provided by A. Fukuda (Tokyo Institute of Technology) and H. T. Nguyen (CNRS).

[34] De Vries, Acta Crystallogr. **4**, 219 (1951).

[35] For a review on optics of CLC, see S. Chandrasekhar, *Liquid Crystals,* 1st ed. Cambridge Monographs on Physics (Cambridge University Press, London, 1977).

[36] C. Oldano, Phys. Rev. Lett. **53**, 2413 (1984).

[37] H. L. Ong, Phys. Rev. A **37**, 3520 (1988).

[38] F. Beaubois and J. P. Marcerou (unpublished).

[39] J. D. Bunning, D. A. Crellin, and T. E. Faber, Liq. Cryst. **1**, 37 (1986).

[40] M. Glogarova, H. Sverenyak, H. Takezoe, and A. Fukuda, Liq. Cryst. **14**, 463 (1993).

[41] In liquid camphor, ORP is about 0.5° mm^{-1}.

[42] E. I. Demikhov, V. K. Dolganov, and V. M. Filev, JETP Lett. **37**, 361 (1983).

[43] J. D. Rosenzweig and P. J. Collings, Phys. Rev. E **47**, 1876 (1993), and the reference therein.

[44] H. Takezoe *et al.*, Ferroelectrics **58**, 55 (1994).

[45] S. A. Pikin and M. A. Osipov, in *Ferroelectric Liquid Crystals: Principles, Properties and Applications* (Gordon and Breach, New York, 1991), p. 249.

[46] M. M. Wittebrood, Th. Raising, and I. Musevic (unpublished).

[47] G. S. Iannacchione and D. Finoletto, Phys. Rev. Lett. **69**, 2094 (1992).

[48] P. Cluzeau (private communication).

[49] O. Mondain-Monval, H. J. Coles, J. R. Lalanne, and J. P. Marcerou, Phys. Rev. E **47**, 2201 (1993).

[50] O. Mondain-Monval, H. J. Coles, T. Claverie, J. R. Lalanne, J. P. Marcerou, and J. Philip, J. Chem. Phys. **101**, 6301 (1994).